The effect of graphene nanoplatelets on the thermal and electrical properties of aluminum nitride ceramics

Irem Nur Gamze Simsek[1], Andrés Nistal[2#], Eugenio García[2], Domingo Pérez-Coll[2,3], Pilar Miranzo[2] and María Isabel Osendi[2*]

[1]Bulent Ecevit University, Incivez, 67100 Zonguldak, Turkey

[2]Institute of Ceramics and Glass (ICV), CSIC, Kelsen 5, 28049 Madrid, Spain

[3]Nanotechnology Research Division, Centre for Mechanical Technology and Automation, Department of Mechanical Engineering, University of Aveiro, 3810-193, Aveiro, Portugal

Abstract

The thermal conductivity (κ) of AlN (2.9 wt. % of Y_2O_3) is studied as a function of the addition of multilayer graphene (from 0 to 10 vol. %). The κ values of these composites, fabricated by spark plasma sintering (SPS), are independently analyzed for the two characteristic directions defined by the GNPs orientation within the ceramic matrix; that is to say, perpendicular and parallel to the SPS pressing axis. Conversely to other ceramic/graphene systems, AlN composites experience a reduction of κ with the graphene addition for both orientations; actually the decrease of κ for the in-plane graphene orientation results rather unusual. This behavior is conveniently reproduced when an interface thermal resistance is introduced in effective media thermal conductivity models. Also remarkable is the change in the electrical properties of AlN becoming an electrical conductor (200 S m^{-1}) for graphene contents above 5 vol. %.

1. Introduction

#Presently at School of Mechanical and Aerospace Engineering, Queen´s University Belfast, UK.

Aluminum nitride (AlN) is an interesting dielectric material since it owns a very high thermal conductivity (κ); hence, AlN ceramics are attractive for systems requiring fast heat release, in particular, for packaging of high power electronics and for light emitting diode arrays[1-2]. The high thermal conductivity of AlN is very sensitive to minor contents of impurities, particularly oxygen, as well as to the presence of porosity. Consequently, this ceramic is often sintered under high temperatures and loads, with small additions of sintering aids, typically Y_2O_3, which promotes densification through liquid-phase formation and, on cooling, forms yttrium aluminate phases that act as oxygen gettering agents[3]. The room temperature κ values of sintered AlN ceramics are normally in the range[4] of 30-270 W m^{-1} K^{-1}, evidently below that of pure single crystals[5] (320 W m^{-1} K^{-1}). Current assisted densification methods like the Spark Plasma Sintering (SPS) allow complete densification of AlN ceramics at temperatures as low as 1600 °C without using sintering aids[6], although κ of such material reached a moderate value of 56 W m^{-1} K^{-1}.

Studying the influence of graphene additions on the thermal conductivity of AlN ceramics, considering that both materials separately are very good thermal conductors, results interesting not only from the academic point of view but also because the practical interest in areas like thermal management, micro and nano- electromechanical systems (MEMS, NEMS), microwave filters, or for light emitting diodes (LED)[7-8]. Furthermore, the effect of graphene additions on the dielectric nature of AlN ceramics is a critical issue to be considered as it could restrict some applications, particularly those concerning electronic packaging, although it could prompt alternative uses (like for LED or MEMS).

Graphene based nanostructures are prominent reinforcements for ceramics[9,10], afford excellent wear resistance characteristics[11,12] and also provide good electrical

conductivity to dielectric matrices[13-14] when present in concentrations above the percolation limit. Surprisingly, the effect of graphene fillers on κ has been by far less addressed, in particular, we can mention the works on Si_3N_4 [15-16], Al_2O_3 [17-18], SiC [19-20] and Y-ZrO_2 [21] composites, always reporting important reductions of κ, except for measurements done in the direction coincident with the graphene plane[15-18,20] in the oriented nanostructures within the composites. Now, regarding AlN ceramics we can mention very few works, which also state reductions of κ with the graphene additions, specifically for the through-plane orientation. In fact, Yun et[22] al. observed decrease of κ from 90 down to 40 W m^{-1} K^{-1} for the 10 vol. % addition of graphene nanoplatelets (GNP) in composites of AlN (plus 2 wt. % Y_2O_3) prepared by hot pressing at 1850 °C in N_2 atmosphere for 1 h. In the same way, Xia el al.[23] reported decreases of κ from 92.5 (AlN) to 37.4 W m^{-1} K^{-1} when adding graphene oxide (GO) that became reduced (rGO) during densification in the SPS at 1550–1600 °C (~3 vol. % rGO composite). Although rGO results an excellent reinforcement for ceramics[9-10,23], it has the disadvantage of its quite low thermal conductivity, for example, a value of κ ~ 0.2 W m^{-1} K^{-1} has been stated for thermally reduced rGO films at 1000 C for through-plane orientation[24], which is one order of magnitude lower than the through-plane thermal conductivity estimated for pristine GNPs, ~6-10 W m^{-1} K^{-1} [20]. Actually, only one report[25] gives κ values for the in-plane heat flow situation of GNP/AlN (with 5% wt.Y_2O_3) composites (hot pressed at 1900 °C for 2h), showing an important decrease from 135 (bare matrix) to 50 W m^{-1} K^{-1} (10 wt.% GNP composite), close to the results they reported for the through-plane orientation.

In the present work, we address the thermal conductivity of AlN (plus 2.9 wt.% Y_2O_3) ceramics with GNP additions, from 0.5 to 10 vol. % densified by SPS, measuring room

temperature κ values for the two characteristic directions defined by the GNPs orientation. The use of GNPs was preferred due to its essentially higher κ as compared to GO sheets; besides, densification by the SPS method was selected as it allows the employ of coarse AlN powders, thus reducing the amount of available surface oxygen. Present data are discussed using simple thermal resistance model and comparing with published κ data for alike materials, demonstrating that this model does not predict the trend for the in-plane situations. Conversely, the effective media conductivity models with certain interfacial thermal resistance gives a reasonable approximation the thermal conductivity of graphene /AlN composites.

2. Experimental

High purity AlN powders synthesized by high temperature self-propagating synthesis (SHS-España), Y_2O_3 (H.C. Starck, Germany) and GNP powders (XG Sciences, USA) were employed in this study. AlN powders have a median particle size (d_{50}) of 11.3 μm and Y_2O_3 powders show d_{50} of 1.0 μm and XG nanoplatelets have a nominal thickness of 5-10 nm and a lateral size of the order of 5 μm. The size of AlN powders was reduced by milling for 4 hrs in a lab scale attritor using ZrO_2 balls -2 mm diameter- as grinding media and isopropyl alcohol as milling fluid. The d_{50} of AlN powders measured by laser scattering (Mastersizer S, Malvern) after 4 h of milling was 1.1μm and the oxygen content was 1.31 wt.% as measured by the hot gas extraction technique (TC-436, LECO). Y_2O_3 powders were added in the proportion of 2.9 wt.% and homogenised by 1h of attrition milling. GNPs were separately dispersed in isopropyl alcohol in concentration of 2 mg/mL and bath sonicated for 1 hr. Next, both suspensions were mixed together and sonicated at 360 W for 2h in given proportions corresponding to 0.5, 5 and 10 vol. % GNPs. Alcohol was removed in a rotary evaporator and next the

powder mixtures were oven dried at 120 °C. Labels and conditions for each powder mixtures are shown in Table 1.

Table 1. Labels for the different powder mixtures

Matrix	**Amount of GNPs (vol %)**	**Label**
AlN – 2.9 wt% Y_2O_3 (~ 4 vol%)	0	A3Y
	0.5	A3Y0.5GNP
	5	A3Y5GNP
	10	A3Y10GNP

Once dried, compositions were put into a 20 mm diameter graphite die and sintered in the SPS equipment (Dr. Sinter, SPS-510CE, Japan). Sintering conditions consisted of uniaxial pressure, 50 MPa, 1700-1750 °C of maximum temperature for 5 minutes and N_2 atmosphere. Density, ρ, of the specimens was measured by the Archimedes' water immersion method. Porosity was assessed by the ratio of measured density to the theoretical density as estimated by rule of mixtures using the following densities for each phase, ρ_{AlN}=3.26 gcm^{-3}, ρ_{Y2O3}= 5.01 gcm^{-3} and ρ_{GNP}=2.2 gcm^{-3}. Phase analyses were identified by X-Ray diffraction (XRD) methods (Bruker, D8 Advance, USA) on the sintered bulk specimens. Raman spectroscopy analyses were accomplished using a confocal Raman-AFM spectrometer (Alpha300, WItec, Germany) with the 532 nm laser wavelength excitation in backscattering configuration. Raman scans of 100 x 100 pixels and 0.1 ms of integration time were recorded on polished areas of 20 x 20 μm^2.

Observation of the fresh fracture surfaces was performed by field emission scanning electron microscopy (FESEM, S-4700 Hitachi, Japan). Images of scanning-transmission microscopy with high-angle annular dark-field (STEM-HAADF) and high resolution transmission electron microscopy (HRTEM) were done in a Tecnai G2-F30 Field

Emission Gun microscope, operated at 300kV and a JEOL 2100 operating at 200 KV with energy dispersive X-Ray diffractometer attachment (EDS). The thin specimen (A3Y5GNP) was prepared by focussed ion beam (FIB) method (Helios NanoLab 650, FEI Company, USA).

Through-plane (direction parallel to the SPS pressing axis) and in-plane (radial direction of the specimens) thermal diffusivity (α) measurements were done by the laser flash method (Thermaflash 2200, Holometrix-Netzsch, Germany). Thermal diffusivity was measured as function of temperature -from RT to 500 °C- in Ar for the through-plane orientation in square specimens of 8.8 mm of edge and ~1mm thick. In-plane α measurements were done at room temperature using a special sample holder described elsewhere[15]. Data represent the average of five measurements. The specific heat (Cp) as a function of temperature was estimated by the rule of mixtures from the chemical composition and the heat capacity data of each phase[26] (see supplementary information, S1). Thermal conductivity, κ, was calculated from α, ρ and C_p according to the following expression:

$$k = \alpha . \rho . C_p \quad (1)$$

Error bars in the κ plots represent the estimated accuracy of the laser flash technique - about 7% - in the case of the through-plane data, and the standard deviation of the values for the in-plane measurements.

The electrical properties at room temperature were studied by Impedance Spectroscopy in the range of 10^{-1}-10^{6} Hz with an ac amplitude of 250 mV, using a potentiostat/galvanostat (Autolab PGSTAT302N with a FRAII module, Metrohm, Switzerland). The electrical field was applied over the external planar surfaces of the square specimens (~8 mm edge by 1 mm thick) through two symmetrical circular Ag

electrodes by means of Ag wires attached by electroconductive paste (Electrolube, ERSCP03B).

3. Results and discussion

All the specimens reached densities within 97.8-99.9 % of the theoretical (Table 1). The addition of 10 vol.% GNPs faintly reduced the relative density achieved when compared to bare AlN, accordingly, the sintering temperature was raised to 1750°C for this composite.

Table 1. Density of the samples

A3Y		**A3Y0.5GNP**		**A3Y5GNP**		**A3Y10GNP***	
ρ (gcm^{-3})	ρ/ρ_{th} (%)	ρ (gcm^{-3})	ρ/ρ_{th} (%)	ρ (gcm^{-3})	ρ/ρ_{th} (%)	ρ (gcm^{-3})	ρ/ρ_{th} (%)
3.25	99.1	3.25	99.9	3.20	99.1	3.11	97.8

*Sintering temperature of 1750°C

The recorded crystalline phases are the same for all the materials; precisely, hexagonal AlN as the major phase, a small fraction of yttrium aluminum garnet (YAG, $Y_3Al_5O_{12}$) and characteristic reflections that correspond to hexagonal carbon (see example of the XRD patterns in supplementary information S2).

The grain size of AlN matrix is not much affected by the presence of platelets as some representative images of the polished microstructures of A3Y and the A3Y5GNP materials evidence (see supplementary information S3), all materials show hexagonal grains with sizes typically in the range of 3-4 μm. The observation at higher magnification, in fracture mode, offers a very clear representation of the microstructure of these materials, as Fig. 1 illustrates.

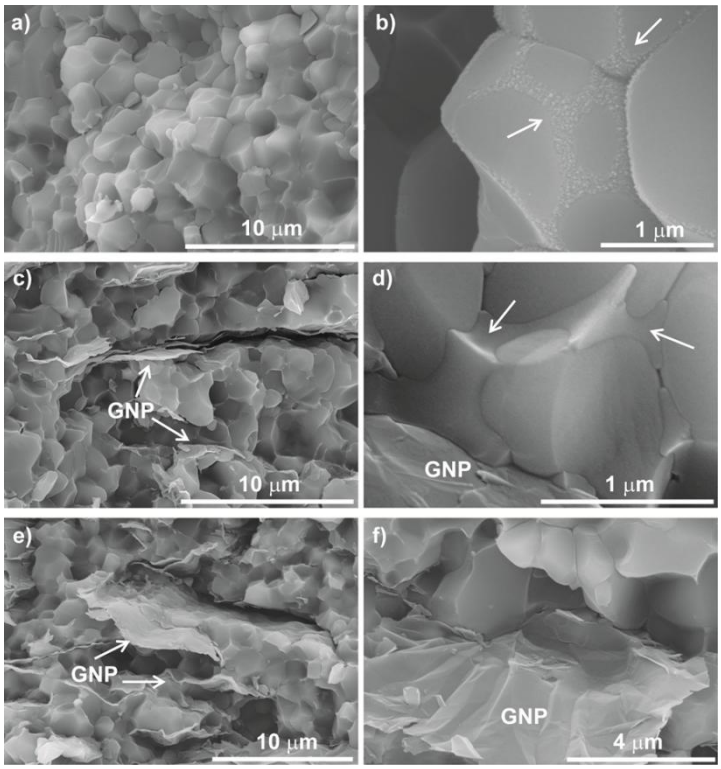

Figure 1. SEM microstructure of fracture surfaces for A3Y (a,b) A3Y5GNP (c,d) and A3Y10GNP (e,f). The presence of GNP is seen in (c,d,e,f), along with the grain boundary phase at grain edges in AlN (b) and in triple points (d).

We typically see round edge hexagonal shaped grains (Fig. 1a-f), a white color phase that mostly concentrates at triple points (pointed by arrows in Fig. 1d) and a grain boundary phase along the grain edges (enlarged in Fig. 1b). The GNPs show a distinct alignment -with the graphene plane perpendicular to the SPS loading axis (Fig. 1 c,e) - and also they seem to follow quite precisely the contours of the AlN grains producing ripples (Fig.1c,e,f). Besides, we can observe fluctuating thickness of platelets due to frequent piling-up and the presence some platelets with very large lateral size (> 4 μm, Fig. 1c,e,f).

A general view in STEM mode (Fig. 2a) of the A3Y5GNP composite evidences the round edge AlN grains of 1-3 μm and the corresponding HAAD image (Fig. 2b) clearly

reveals the grain boundary phase (white phase) and GNPs (black features) due to the enhanced atomic contrast.

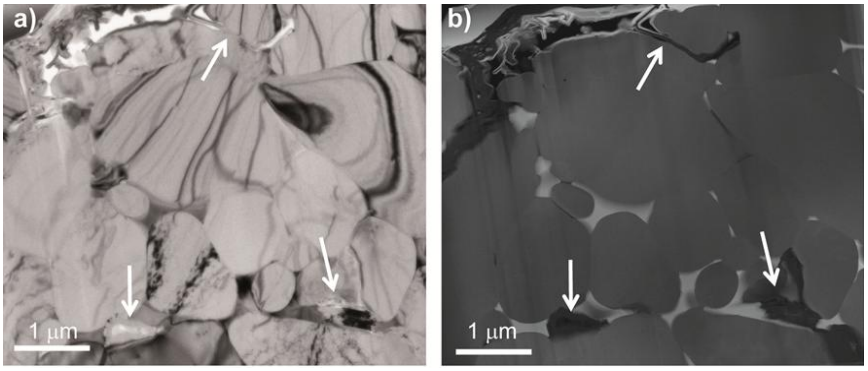

Figure 2. Corresponding images of A3Y5GNP composite in (a) STEM and (b) HADDF modes. The arrows point to GNP locations. Image (b) permits a clear identification of the grain boundary phase by the white contrast and GNPs as the dark phase.

The HRTEM images (Fig. 3a,b) allow perfect observation of the crystalline nature of this secondary phase at triple points, which according to EDS microanalysis performed in the point signaled in Fig. 3a contains Y, Al and O atoms, in a ratio (52 O:34 Al:14 Y) compatible with the YAG phase (also identified by XRD methods). This phase penetrates along the AlN/AlN interfaces as well creating a grain boundary phase of few nm as it can be observed (Fig. 3 c,d), whereas, the GNP/AlN interface shows a direct bond (Fig. 3 e,f). The atomic line profiles across both interfaces displays their differences; the concentration of Al, Y and O atoms at AlN grain boundaries is obvious, whereas the GNP/AlN interface shows typical atomic profiles of direct contact boundaries with a narrow zone of mutual solid solution (ss) (see supplementary information S4).

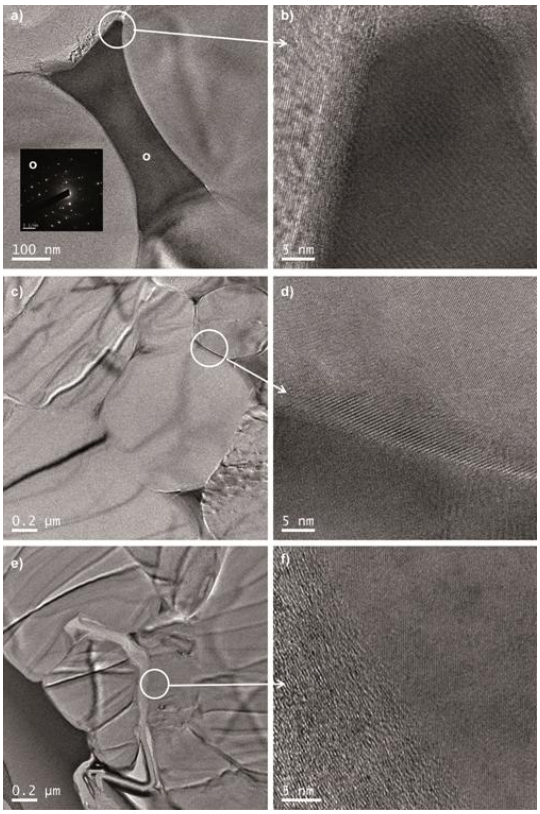

Figure 3. TEM/HRTEM images of A3Y5GNP composite showing a crystalline triple point region (YAG phase) and the corresponding SAD pattern (a); an enlarged view of the encircled area in a) corresponding to the YAG/GNP interface (b); zone with AlN grains (c) and a higher magnification image indicating the occurrence of a crystalline boundary phase of few nm between the AlN crystals (d); region displaying the GNP twisting around AlN grains (e) and a closer view of the encircled area in e) indicating the good contract between GNP and AlN phases (f).

Representative Raman features of these materials are displayed in Fig. 4. The AlN phase is Raman active[27] with characteristic peaks at 611, 661, 670 and 915 cm^{-1} that correspond to the modes $A_1(TO)$, E_2 (high), $E_1(TO)$ and $E_1(LO)$. Fig. 4d shows the average spectrum of A3Y0.5GNP composite –cross section view- where some of the AlN bands are identified together with the typical D, G and 2D bands of graphene materials.

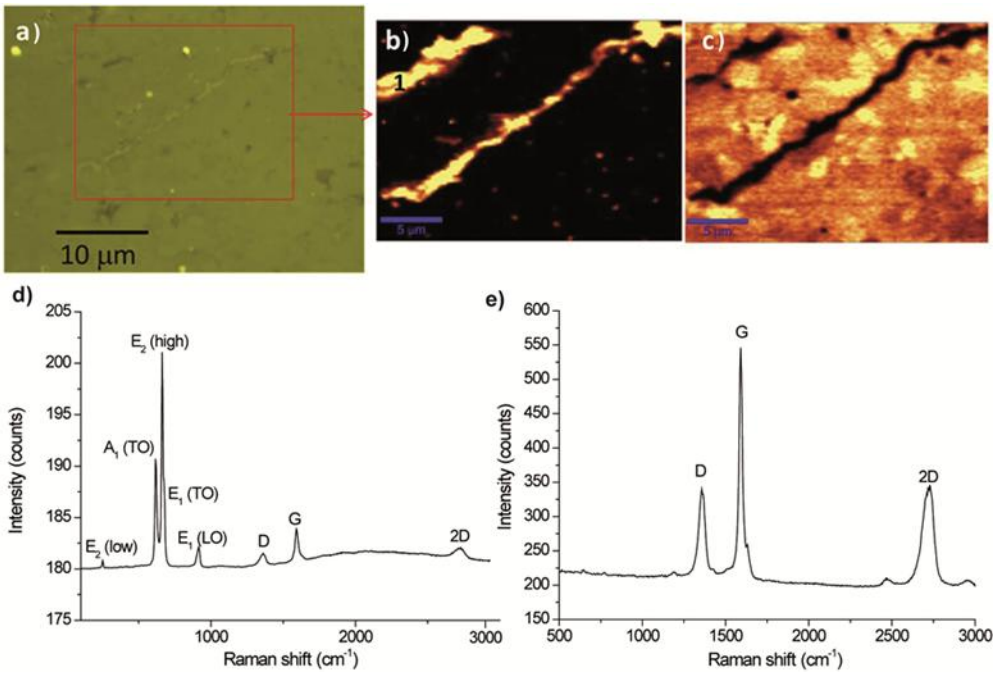

Figure 4. Optical image of A3Y0.5GNP composite (a) and corresponding views of boxed zone in a) filtered by the G band of GNPs (b) and by the frequency interval of the AlN triplet (A1, E2, E1 bands) in (c). Average Raman spectrum of boxed region is plotted in (d) and example of GNP point spectrum (e) corresponding to the point marked as 1 in (b).

The image created by filtering the G band of graphene (Fig 4b) shows the edge view and the distinct alignment of GNPs; correspondingly, the image filtered by the frequency window of the AlN triplet (600-680 cm^{-1}) reproduces the negative image where AlN grains are readily identified showing different brightness due to different crystal orientations (Fig. 4c). The intensity ratio of bands I_D/I_G depends on the type of image -side or top view of GNPs- but typically stays in the range of 0.5-0.65, which is similar to the range of values reported for edge side patterns of different GNP-ceramic composites[14,17].

The electrical conductivity (σ_e) of the blank material (A3Y) falls under the detection limit -estimated from the beginning of the very high resistive arcs in the impedance

spectra- whereas composites with 5 and 10 vol. % GNPs are electrically conductors, reaching a top value close to 200 $S \cdot m^{-1}$ for the last composite (Fig. 5).

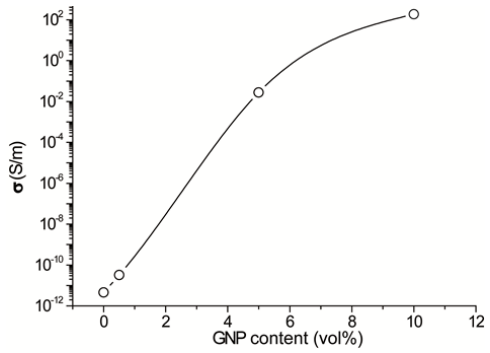

Figure 5. Plot of ac electric conductivity data vs GNP content in the AlN composites

Compared to published results for dielectric matrices, the top σ_e of present is similar to that reported by Yun et al. [22] for AlN with 10 vol. % of graphene nanosheets (GNS) and only overpassed by data of Fan et al[28] for GNS/Al_2O_3 composites (~2000 S m^{-1} for 10 vol % GNS). As the A3Y5GNP composite shows a measurable σ_e of the order of 10^{-2} $S \cdot m^{-1}$ conversely to alike processed GNP/Si_3N_4 composites, a lower percolation limit (<0.05) is presently inferred. The lower percolation limit might be a topological effect induced by the larger grain size of the AlN matrix – d~3 μm compared to 0.3 μm of the referred Si_3N_4 composites- as GNP sheets locate along grains boundaries.

The results of thermal diffusivity and conductivity (Fig. 6) as a function of the GNP content indicate interesting features regarding specimen orientation with respect to the heat flow. The room temperature trough-plane α and κ values (Fig. 6 a,b) decrease progressively with the volume fraction of nanoplatelets as it has been observed for AlN and other matrices with graphene based fillers[15-21]. Interestingly, for the in-plane orientation α and κ data also decrease with the GNP fraction (see Fig. 6 a,b). The κ ratio between the in- and trough-plane orientations in these composites, $\kappa_{in}/\kappa_{trough,}$

increases with the filler content reaching a top value of 1.9 for the 10 vol.% of GNPs following same trend as observed in other ceramic composites for the same filler range[15,20].

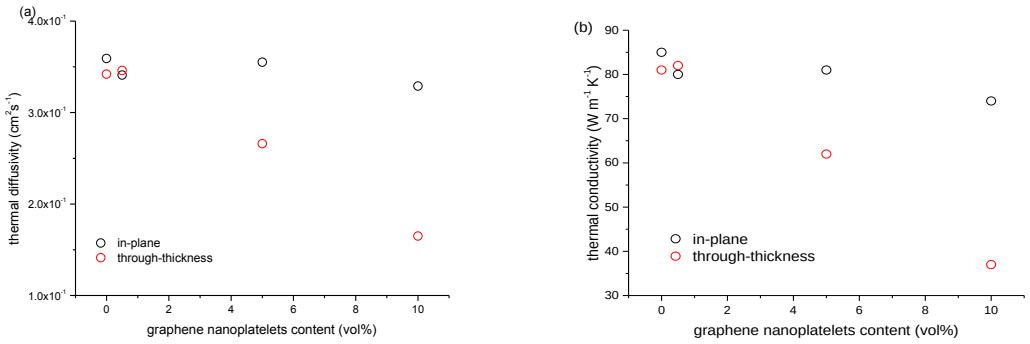

Figure 6. Plots of α (a) and κ (b) for all the materials and the two tested orientations through-thickness and in-plane.

We can make the exercise of comparing present κ data with reported data from the literature for various AlN materials of with graphene additions[22,23,25]. Accordingly, all these values are plotted in Fig. 7 for the heat flowing in the though-plane direction, the solid lines in the figure representing the κ fittings performed with the simple thermal resistance model[29] for series resistances configuration. Corresponding κ data for the bare matrix were used for each composite fitting and values of through-plane κ of the GNP fillers were estimated from the best fitting to each experimental data set, which varied in the range 2.5-7 W m^{-1} K^{-1} depending on the composite set (see Fig. 7). Here, the interfacial thermal barrier resistance between GNPs and the ceramic matrix is assumed to be linked to κ of the graphene filler. The lowest value of 2.5 Wm^{-1} K^{-1} was ensued for κ_{rGO} obtained from the best to the rGO/AlN data of Xia et al[23], whereas present data and those of Yun et al[22] for AlN with GNP fillers are reasonable fitted using a through-plane κ_{GNP} of 7 W m^{-1}K^{-1}. Conversely, data of Rutkowski et al.[25]

required a κ_{GNP} of 4 $Wm^{-1}K^{-1}$ to acceptably approximate their results. This range of conductivities are ≤below κ_{GNP} estimated for comparable Si_3N_4 and SiC composites[15,20] (~7 – 10 $Wm^{-1}K^{-1}$) and they are even lower than typical data for the through-plane conductivity of pyrolytic graphite[30], hence being hints than the contact thermal resistances in the graphene/AlN system are rather important.

Data for the in-plane direction are very scarce as we can see in Fig 8. where present data are plotted with just those of Rutkowsky et al.[25] using the same model but for the parallel configuration, and using a value of 150 Wm^{-1} K^{-1} for the in-plane κ_{GNP} – that proved good matching for thermal conductivity results of SiC and Si_3N_4 composites containing graphene nanoplatelets[15,20]. We see that in-plane κ data for AlN composites are not fitted by this model at all; in fact, suitable fitting to present GNPs composites data would require a κ_{GNP} ~ 8 W m^{-1} K^{-1} for the in-plane orientation, which is rather improbable as it is a figure representative of amorphous carbon[30]. Although certain increase of the defects band (I_D/I_G~0.65) occurs in the specimens, this number stays within the range of figures reported for GNP composites processed by SPS[14,17].

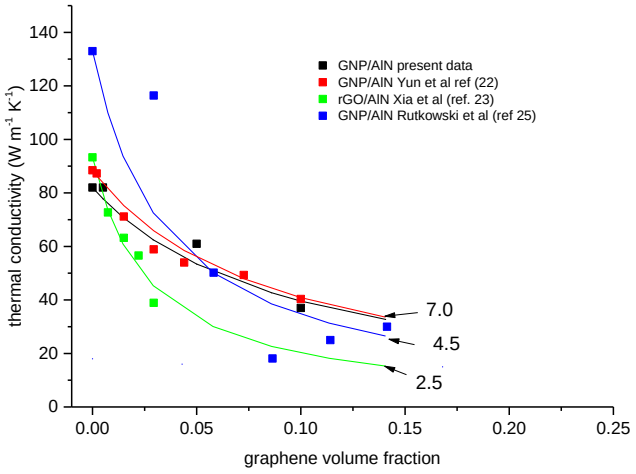

Figure 7. Plot of through- plane κ for present materials vs GNP volume fraction jointly with published data redrawn from refs [22], [23] and [25] for various types of graphene/AlN composites. Lines correspond to fittings to the thermal resistance model for each composite set, and the number next to lines indicates the κ_{GNP} used in the fittings.

On the other hand, the unexpected $\kappa_{in\text{-}plane}$ reduction could be attributed to the matrix. To explore this conjecture, Raman spectra were carefully checked looking for a possible line broadening, in particular of the E_2(low) Raman band of AlN. Actually, this type of broadening associated to the presence of oxygen impurities has been linked to a reduction of the phonon mean free path[31], which directly relates to the thermal conductivity[32]. No representative evidence of broadening of line E_2 was seen – measured after deconvolution of the AlN triplet and fitting to a lorentzian function, see example in supplementary information S5.

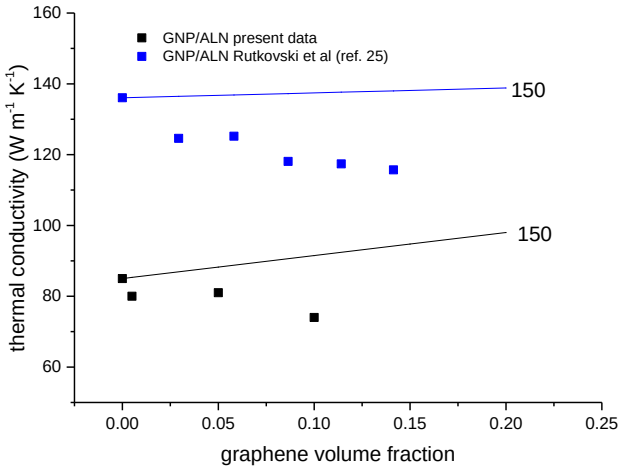

Figure 8. Plot of in- plane κ for present materials vs GNP volume fraction jointly with published data redrawn from ref [25] for graphene/AlN composites. Lines correspond

to the thermal resistance model for each composite set using the number next to lines indicates the κ_{GNP} used in the fittings.

Alternatively, the thin interaction zone (ss) at the GNP/AlN interface could be held responsible for the large thermal resistance, and thus explaining the declining κ independently of orientation. Furthermore, this effect would be intensified as the number of these interfaces augments - i.e. 10 vol% GNP composites- as experimentally observed (Fig. 7 and 8). To examine this point, we can apply the models for effective media thermal conductivity of particulate composites with interfacial thermal resistances[33]. The expression for laminated flat plates[33] of 100 nm of thickness oriented perpendicular to the X_3 axis was used for the through-plane condition:

$$K_3 = K_p K_m / [K_p - f(K_p - K_m - \alpha K_p)] \quad (2)$$

whereas for the in-plane condition the correct experimental trend was reproduced using the expression for spheres[33] (with same characteristic length of 100 nm) [33]:

$$K_{eff} = K_m \{K_p(1+2\alpha) + 2K_m + 2f(Kp(1-\alpha) - K_m)/[K_p(1+2\alpha) + 2K_m - f(K_p(1-\alpha) - K_m)]\} \quad (3)$$

K_m and K_p are thermal conductivities of matrix and particle, respectively; α is dimensionless parameter related with the interface thermal resistance (Rc) and the particle size in the given orientation (d) by the expression $\alpha = K_m R_c/d$, and f is the volume fraction of particles. The first expression fits to present experimental results for through-plane conductivity, whereas the second expression matches the in-plane conductivity data using in both cases a contact thermal conductance (h_c) of~ 3 x 10^8 W m^{-2} K^{-1} for the AlN/GNP interface Table 2 includes the values obtained using these

equations and the deviation from the experimental data, showing that this new model reasonably reproduces the experimental κ values for both orientations.

Table 2. Comparison between the effective thermal conductivity K_{eff} (W m^{-1} K^{-1}) and experimental values K_{exp} for present GNP/AlN composites. Ratio between κof matrix and GNPs for given orientations, volume fraction, f, and the interface thermal conductance parameter h_c used for calculations are shown in the table.

$\kappa_{GNP}/\kappa_{ALN}$	f	h_c (Wm^{-2} K^{-1})	K_{eff} (Wm^{-1} K^{-1})	K_{exp} (W m^{-1} K^{-1})	Difference (%)
In-plane					
1.764	0.1	2.83E+08	77.1	74	4.3
1.764	0.05	2.83E+08	81.0	81	0.04
1.764	0.005	2.83E+08	84.5	81	4.4
Through-plane					
0.121	0.1	2.86E+08	40.8	37	10.4
0.121	0.05	2.86E+08	54.5	61	-10.5
0.121	0.005	2.86E+08	78.0	82	-4.7

This interface thermal conductance is the effect of the graphene thermal coupling with a substrate owing to the differences in the phonon density of states[30]; in fact, calculations and experiments on the graphene- SiO_2 coupling gave interface thermal conductance[30] of ~2,5 x10^7 $Wm^{-2}K^{-1}$, with large variations measured from specimen to specimen; therefore, the estimated h_c value for present composites seems reasonable.Consequently, the thermal conductivity in graphene/AlN composites seems controlled by the occurrence of strong atomic interaction at the GNP/AlN interface – also supported by HRTEM observations- altering the possible phonon modes.

Finally, the change of κ with temperature shows the characteristic gradual decrease[32] represented by a function of the type A T^{-B} (A and B are fitting parameters and T the absolute temperature), as it can be seen in Fig. 9. The decline of κ with temperature

becomes smoother as the amount of GNPs increases because the parameter B lessens progressively: 0.65 (A3Y), 0.52 (A3Y5GNP) and 0.34(A3Y10GNP). Therefore, it seems that the usual predominance of dispersive effects when the temperature raises attributed to phonon-phonon scattering is modulated in these composites by additional phonon-defect scattering events -likely at the GNP/AlN interfaces- at least for the intermediate temperatures.

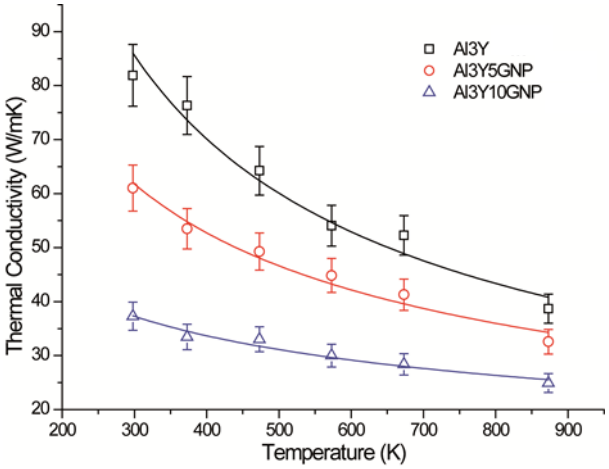

Figure 9. κ vs temperature for the indicated composites, lines are best fittings to functions of the type $A\ T^{-B}$.

4. Conclusions

The addition of GNPs to a high thermal conductor like AlN produces a sharp decrease of κ when heat flows in a direction perpendicular to the nanoplatelets. A smother decline for the in-plane direction is observed, which is a reverse trend to that stated for other GNP/ceramic composites. The reduction of κ for both orientations is reasonably fitted using the effective media approach and introducing a thermal contact resistance at the AlN/graphene interface ascribed to a strong coupling between both phases. The high directionality of heat conduction for these composites with κ ~80 W m^{-1} K^{-1} for the in-plane direction and half this value for the through plane can have interest for

applications requiring fast heat release at specific directions as for example in thermal interface materials. Additionally, for graphene contents ≥ 5 vol. %, these composites develop a high electrical conductivity and therefore could produce useful materials for applications such as LEDs or MEMs.

Acknowledgements

The Present work was financed by CSIC (Spain) under project PIE201360E063 and MINECO (Spain) with project MAT2015-67437-R. One of the authors (I. Simsek) greatly acknowledges the Erasmus+ Internship mobility program delivered by Anadolu University for financing her stay in the ICV-CSIC. Dr. Pérez-Coll is acknowledged to the FCT in Portugal for financial support by a BPD grant (SFRH/BPD/112282/2015). The assistance of the Laboratorio de Microscopías Avanzadas (LMA) from the Instituto de Nanociencia de Aragón (INA) (Universidad de Zaragoza) in the HRTEM observations and specimen preparation by FIB method is acknowledged. The support of the Transmission Electron Microscopy Unit of the Institute of Catalysis and Petrochemistry (CSIC) is also recognised.

References

[1] Lostetter AB, Barlow F, Elshabini A. An overview to integrated power module design for high power electronics packaging. Microelectron Reliab 2000;40 (3):365–79. http://dx.doi.org/10.1016/S0026-2714(99)00219-X

[2] Christensen A, Graham S. Thermal effects in packaging high power light emitting diode arrays. Appl Therm Eng, 2009;29(2–3):364–71. http://dx.doi.org/10.1016/j.applthermaleng.2008.03.019

[3] Sainz de Baranda P, Knudsen AK, Ruh E. Effect of yttria on the thermal conductivity of aluminum nitride. J Am Ceram Soc 1994;77(7):1846 – 50. http://dx.doi.org/10.1111/j.1151-2916.1994.tb07060.x

[4] Lee RR, Development of high thermal conductivity aluminum nitride ceramic, J Am Ceram Soc 1991;74(9):2242 –49. http://dx.doi.org/10.1111/j.1151-2916.1991.tb08291.x

[5] Slack GA. Nonmetallic crystals with high thermal conductivity. J Phys Chem Solids 1973;34(2):321 – 35. http://dx.doi.org/10.1016/0022-3697(73)90092-9

[6] Qiao L, Zhou H, Li C. Microstructure and thermal conductivity of spark plasma sintering AlN ceramics. Mater Sci Eng B 2003;99(1– 3):102 – 5. http://dx.doi.org/10.1016/S0921-5107(02)00429-4

[7] Dubois MA, Muralt P. Properties of aluminum nitride thin films for piezoelectric transducers and microwave filter applications. Appl. Phys. Lett. 1999;74(20):3032–4. http://dx.doi.org/10.1063/1.124055

[8] Taniyasu Y, Kasu M, Makimoto T. An aluminum nitride light-emitting diode with a wavelength of 210 nanometres. Nature 2006;441(7091);325–8. http://dx.doi.org/10.1038/nature04760

[9] Ramirez C, Miranzo P, Belmonte M, Osendi MI, Poza P, Vega-Diaz SM et al. Extraordinary toughening enhancement and flexural strength in Si3N4 composites using graphene sheets, J Eur Ceram Soc 2014;34(2):161–9. http://dx.doi.org/10.1016/j.jeurceramsoc.2013.08.039

[10] Belmonte M, Nistal A, Boutbien P, Román-Manso B, Osendi MI, Miranzo P. Toughened and strengthened silicon carbide ceramics by adding graphene-based fillers. Scripta Materialia, 2016;113:127–30. http://dx.doi.org/10.1016/j.scriptamat.2015.10.023

[11] Belmonte M, Ramirez C, González-Julián J, Schneider J, Miranzo P, Osendi MI. The beneficial effect of graphene nanofillers on the tribological performance of ceramics. Carbon 2013;61:431–5. http://dx.doi.org/10.1016/j.carbon.2013.04.102

[12] Kim HJ, Lee SM, Oh YS, Yang YH, Lim YS, Yoon DH et al. Unoxidized graphene/alumina nanocomposite: fracture- and wear-resistance effects of graphene on alumina matrix. Sci Rep 2014;4:5176. http://dx.doi.org/10.1038/srep05176

[13] Wang K, Wang Y, Fan Z, Yan J, Wei T. Preparation of graphene nanosheet/alumina composites by spark plasma sintering. Mater Res Bull 2011;46(2):315–8. http://dx.doi.org/10.1016/j.materresbull.2010.11.005

[14] Ramirez C, Figueiredo FM, Miranzo P, Poza P, Osendi MI. Graphene nanoplatelet/silicon nitride composites with high electrical conductivity. Carbon, 2012;50(10):3607–15. http://dx.doi.org/10.1016/j.carbon.2012.03.031

[15] Miranzo P, Garcia E, Ramirez C, Gonzalez-Julian J, Belmonte M, Osendi MI. Anisotropic thermal conductivity of silicon nitride ceramics containing carbon nanostructures, J Eur Ceram Soc 2012;32(8):1847–54. http://dx.doi.org/10.1016/j.jeurceramsoc.2012.01.026

[16] Rutkowski P, Stobierski L, Gorny G, Thermal stability and conductivity of hot-pressed Si_3N_4–graphene composites, J Therm Anal Calorim 2014;116(1):321–8. http://dx.doi.org/10.1007/s10973-013-3565-6

[17] Çelik Y, Çelik A, Flahaut E, Suvaci E. Anisotropic mechanical and functional properties of graphene-based alumina matrix nanocomposites. J Eur Ceram Soc 2016;36(8):2075–86. http://dx.doi.org/10.1016/j.jeurceramsoc.2016.02.032

[18] Jankovsky O, Simek P, Sedmidubsky D, Huber S, Pumera M, Sofer Z. Towards highly electrically conductive and thermally insulating graphene nanocomposites:Al_2O_3–graphene, RSC Adv 2014;4(15):7418–24. http://dx.doi.org/10.1039/C3RA45069D

[19] Li Q, Zhang Y, Gong H, Sun H, Li T, Guo X, Ai S. Effects of graphene on the thermal conductivity of pressureless-sintered SiC ceramics. Ceram Int 2015;41(10):13547–52. http://dx.doi.org/10.1016/j.ceramint.2015.07.149

[20] Román-Manso B, Chevillotte Y, Osendi MI, Belmonte M, Miranzo P. Thermal conductivity of silicon carbide composites with highly oriented graphene nanoplatelets. J Eur Ceram Soc. In press. http://dx.doi.org/10.1016/j.jeurceramsoc.2016.06.016

[21] Estili M, Wu WW, Khazaei M, Sakka Y. Mechanically reliable thermoelectric (TE) nanocomposites by dispersing and embedding TE-nanostructures inside a tetragonal ZrO_2 matrix: the concept and experimental demonstration in graphene oxide-3YSZ system. Sci Technol Adv Mater 2014;15(1):014201. http://dx.doi.org/10.1088/1468-6996/15/1/014201

[22] Yun C, Feng Y, Qiu T, Yang J, Li X, Yu L, Mechanical, electrical and thermal properties of graphene nanosheet/aluminum nitride composites. Ceram Int 2015;41(7):8643–9. http://dx.doi.org/10.1016/j.ceramint.2015.03.075

[23] Xia H, Zhang X, Shi Z, Zhao C, Li Y, Wang J et al. Mechanical and thermal properties of reduced graphene oxide reinforced aluminum nitride ceramic composites, Mater Sci Engi A 2015;639:29–36. http://dx.doi.org/10.1016/j.msea.2015.04.091

[24] Renteria JD, Ramirez S, Malekpour H, Alonso B, Centeno A, Zurutuza A et al. Anisotropy of thermal conductivity of free-standing reduced graphene oxide films

annealed at high temperature. Adv Funct Mater 2015;25(29):4664–72. http://dx.doi.org/10.1002/adfm.201501429

[25] Rutkowski P, Kata D, Jankowski K, Piekarczyk W. Thermal properties of hot-pressed aluminum nitride–graphene composites. J Therm Anal Calorim 2016;124(1):93–100. http://dx.doi.org/10.1007/s10973-015-5091-1

[26] Roine A. Outokumpu HSC Chemistry for Windows V 5.11. Outokumpu Research; Pori, Finland, 2002.

[27] McNeil LE, Grimsditch M, French RH. Vibrational spectroscopy of aluminum nitride. J Am Ceram Soc 1993;76(5):1132–36. http://dx.doi.org/10.1111/j.1151-2916.1993.tb03730.x

[28] Fan Y, Wang L, Li J, Sun S, Chen F, Chen L, et al. Preparation and electrical properties of graphene nanosheet/Al_2O_3 composites. Carbon 2010;48(6):1743–9. . http://dx.doi.org/10.1016/j.carbon.2010.01.017

[29] Hasselman DPH, Johnson LF. Effective thermal conductivity of composites with interfacial thermal barrier resistance. J Compos Mater 1987; 21(6): 508–15. http://dx.doi.org/10.1177/002199838702100602.

[30] Balandin AA. Thermal properties of graphene and nanostructured carbon materials Alexander A. Balandin. Nat. Mat. 2011;10(8):569-81. http://dx.doi.org/10.1038/NMAT3064

[31] Lughia V, Clarke DR. Defect and stress characterization of AlN films by Raman spectroscopy. Appl Phys Lett 2006;89:241911. http://dx.doi.org/10.1063/1.2404938

[32] Kingery WD. Thermal Conductivity: XII, Temperature dependence of conductivity for single- phase ceramics. J Am Ceram Soc 1995;38(7):251–5. http://dx.doi.org/10.1111/j.1151-2916.1955.tb14940.x

[33] Nan CW, Birringer R, Clarke DR, Gleiter H. Effective thermal conductivity of particulate composites with interfacial thermal resistance. J. Appl. Phys. 1997;81 (10): 6692-9.
http://dx.doi.org/10.1063/1.365209

Electronic Annex

Click here to download Electronic Annex: Supplementary Information_special issue.pdf